Phase Transition in Cu-Intercalated Misfit-Layer Compounds

Youichi Ohno

Department of Electrical and Electronic Engineering, Faculty of Engineering, Utsunomiya University, 2753 Ishii-machi, Utsunomiya, Tochigi 321, Japan

The Cu-intercalated misfit-layer compounds $Cu_x(MS)_{1+y}$ $(NbS_2)_2$ ($M =$ Ce and Sm), which consist of regularly stacked Cu, MS, and NbS_2 layers with incommensurate intergrowth structure, are studied by means of X-ray photoelectron spectroscopy (XPS) and electron energy loss spectroscopy (EELS). The Nb $N_{2,3}$ inner-shell electron energy loss spectroscopy (ISEELS) spectra and the valence-band XPS spectra show charge transfer from Cu and MS layers to NbS_2 layers. A strong Cu–Nb interaction and a drastic change of the electronic structure are found, which may result from the change of the crystal structure within a NbS_2 sublattice from the 3R polytype at lower Cu concentration to the 2H and/or the 4H polytypes at higher Cu concentration. In the 3R polytype, Nb atoms sit in the center of a trigonal prism with six S atoms at the corners whereas in the 2H and/or the 4H polytypes, all or half of the Nb atoms are surrounded octahedrally by six S atoms. An intercalated Cu layer donates a larger number of electrons to NbS_2 layers than a MS layer at the maximum uptake of $x = 0.67$. Finally, the Nb d_{z^2} band is completely filled with two electrons per Nb atom and the rigid-band model is no longer valid. © 1997 Academic Press

INTRODUCTION

Misfit-layer compounds, which are represented by $(MX)_{1+y}TX_2$ ($M =$ Sn, Pb, Bi, Sb, and rare-earth element; $T =$ Ti, V, Cr, Nb, and Ta; $X =$ S and Se; $y = 0.08$–0.28), were first synthesized by Sterzel (1) in 1966. Afterward, superconductivity was found for some Nb and Ta compounds, although their critical temperatures are as low as those for TX_2 compounds (2). The precise determination of the crystal structure was made by Otero-Diaz *et al.* (3) for $(LaS)_{1+y}CrS_2$ in 1985 and by Wiegers *et al.* (4), Meerschaut *et al.* (5), and Williams and Hyde (6) for other misfit-layer compounds in 1988. These compounds are constructed of MX and TX_2 layers alternately stacked along the c axis, resulting in a one-dimensional superlattice on the atomic scale. Since then, the physical properties and electronic structure of these compounds have been studied extensively in parallel with the discovery of new compounds belonging to the family (7–10). Many experimental results to date show

that they may be regarded not only as incommensurate planar intergrowth compounds with lattice periods which coincide in the b and c directions but not in the a direction but also as intercalation derivatives of layered TX_2 compounds. In misfit-layer compounds, MX layers behave as intercalants and a fractional part of an electron per MX molecule is transferred to TX_2 layers.

Recently, various staging compounds have also been found in which an MX layer is inserted into every second and every third van der Waals gap of a TX_2 lattice (11–15). The remaining van der Waals gaps are unoccupied by an MX layer, so that other foreign atoms and molecules can be additionally intercalated. Thus, this method provides a new technique for preparing multilayer compounds and building one-dimensional superlattices with good quality and with a period longer than that of the pristine compound, although it is still shorter than those of artificial superlattices prepared by means of other methods. Tirado and co-workers (16) and Rouxel and co-workers (17) have succeeded in intercalating Li and Na into second-stage compounds, resulting in the multilayer compounds $M'_x(PbS)_{1+y}$ $(TS_2)_2$ ($M' =$ Li and Na; $T =$ Ti and Nb). However, alkali-metal intercalation derivatives are unstable in the atmosphere. Recently, the present author has succeeded in growing single crystals of $Cu_x(MS)_{1+y}(NbS_2)_2$ ($M =$ Ce and Sm) which are stable in the atmosphere (18). The crystal structure at low Cu concentration is illustrated in Fig. 1, in which we assume that the atomic arrangement and the stacking sequence of NbS_2 layers resemble those of 3R-NbS_2 as confirmed for second-stage misfit-layer compounds (11, 19). We also assume that Cu atoms occupy tetrahedral sites in the van der Waals gaps between two successive NbS_2 layers as confirmed for the Cu-intercalation derivatives of NbS_2 (20) and $NbSe_2$ (21). The repeat distance in the c direction perpendicular to the layers is ~ 18 Å, which is equal to the sum of the repeat distances of bulk $(MS)_{1+y}NbS_2$ and Cu_xNbS_2 and is comparable with those of high-temperature superconducting oxides.

This paper presents X-ray photoelectron spectroscopy (XPS) and electron energy loss spectroscopy (EELS) studies of a phase transition in $Cu_x(MS)_{1+y}(NbS_2)_2$ ($M =$ Ce and
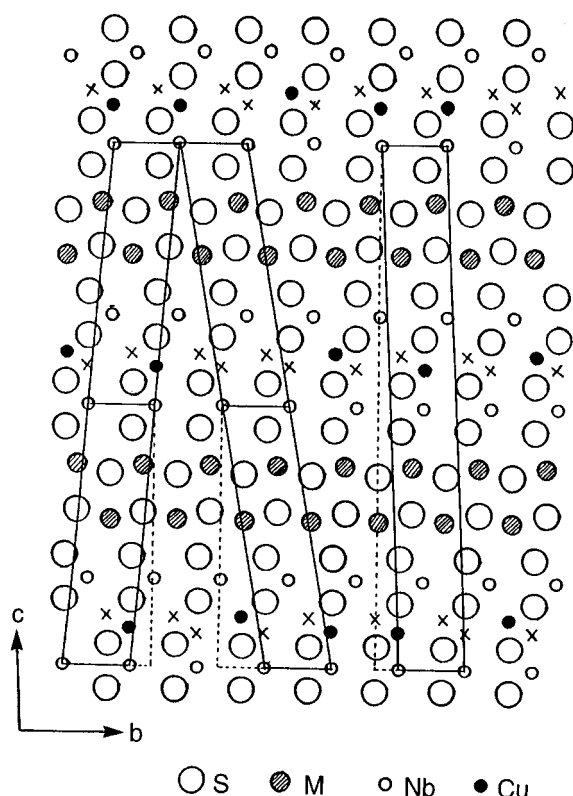
FIG. 1. Crystal structure of Cu-intercalated misfit-layer compounds at low Cu concentration. Solid lines show the unit cells which are given by Meerschaut *et al.* (11) and Terashima (19). Cu atoms occupy tetrahedral sites in the van der Waals gaps between two successive NbS$_2$ layers.

Sm). The next section gives a description of the crystal growth and the X-ray analysis of Cu-intercalated misfit-layer compounds and their XPS and EELS measurements. The XPS and the inner-shell electron energy loss spectroscopy (ISEELS) results are discussed first and four different polytypes are proposed. Then the EELS spectra containing interband transitions and excitation of valence plasmons are discussed.

EXPERIMENTS

Single crystals of the Cu-intercalated misfit-layer compounds Cu$_x$(MS)$_{1+y}$(NbS$_2$)$_2$ are grown from the admixture of Cu and (MS)$_{1+y}$(NbS$_2$)$_2$ by chemical vapor transport reaction. (MS)$_{1+y}$(NbS$_2$)$_2$, the second-stage misfit-layer compounds, are prepared by high-temperature reaction of M_2S$_3$, Nb, and S, which are admixed at the composition ratio of 1:4:7. The resulting compounds are ground into a fine powder in air before being reheated together with Cu and a small amount of iodine added as a transport reagent. The reactions are done in a quartz tube sealed under vacuum. During crystal growth, the temperature gradients of

a two-zone electric furnace are kept at 930 and 880°C. Lamellar crystals are grown in the high and intermediate temperature zones after reaction for 3 weeks. Large single crystals of ca. $5 \times 5 \times 0.01$ mm^3 are used for XPS and EELS measurements.

Powder X-ray diffraction patterns show that the crystals are incommensurate, consisting of alternately stacked MS and Cu$_x$(NbS$_2$)$_2$ layers. For Cu$_x$(CeS)$_{1+y}$(NbS$_2$)$_2$, CeS layers have tetragonal geometry with lattice constants of $a_1 = 5.80$ Å, $b_1 = 5.80$ Å, and $c_1 = (17.90–18.01) \times 2$ Å and Cu$_x$(NbS$_2$)$_2$ layers have hexagonal geometry with lattice constants of $a_2 = 3.35$ Å and $c_2 = (17.90–18.01) \times 2$ Å, where $a_1 = \sqrt{3}a_2$. y is estimated from the relation $y = (2a_2/a_1) - 1 = 0.16$. The number of intercalated Cu atoms is roughly estimated from the lattice expansion along the c axis, which is nearly proportional to the Cu concentration. The repeat distance along the c axis or the half of the c lattice constant increases with Cu intercalation by 0.55–0.66 Å from the value of (CeS)$_{1.16}$(NbS$_2$)$_2$. The repeat distance of (CeS)$_{1.16}$(NbS$_2$)$_2$ is 17.35 Å, which is given by $(c/2)\cos\alpha$, where α is the monoclinic angle. The lattice expansion is comparable with that found for the Cu-intercalated derivative of NbS$_2$ at the maximum Cu concentration of $x = 0.67$. In this case, Cu atoms occupy ca. one-third of two available tetrahedral sites per Nb atom. For Cu$_x$(SmS)$_{1+y}$(NbS$_2$)$_2$, SmS layers have orthorhombic symmetry with lattice constants of $a_1 = 5.76$ Å, $b_1 = 5.79$ Å, and $c_1 = 17.75 \times 2$ Å and Cu$_x$(NbS$_2$)$_2$ layers have hexagonal symmetry with lattice constants of $a_2 = 3.35$ Å and $c_2 = 17.75 \times 2$ Å. The repeat distance increases by 0.56 Å from the value of (SmS)$_{1.19}$(NbS$_2$)$_2$.

Atomically smooth and clean surfaces are prepared by cleavage with adhesive tape, although it is more difficult than previously experienced with the pristine compounds and other layered materials and the resulting surfaces are more active to residual gases. The argon-ion sputtering technique is also used to prepare clean surfaces. However, its use is restricted in the case of heavy surface contamination after long-time measurements, because it disturbs the surface atomic arrangement and results in a surface chemical composition that differs from the bulk one. Auger electron spectroscopy (AES) spectra sometimes show peak shifts due to a charging effect, indicating a small number of free carriers.

The XPS and EELS measurements are carried out with a double-pass cylindrical mirror analyzer (CMA) which is equipped with a normal-incidence electron gun. To optimize the signal to noise ratio and the energy resolution, the pass energy in the CMA is chosen as 15, 25, or 50 eV. The XPS spectra are measured for deeper Cu 2p, Ce 3d, and Sm 3d levels, shallower Nb 4p, Ce 5p, and Sm 5p levels and the valence band. A commercially available dual-anode X-ray tube is employed as an X-ray source, which is operated at 15 kV and 20 mA. The EELS spectra are measured in two

modes; one is the voltage modulation mode and the other is the pulse-counting mode. In the former mode, second-derivative spectra are obtained, using a lock-in amplifier, whereas in the latter mode, the energy distribution curves are allowed at small beam current. In both cases, the data obtained by repeat measurements are stored in a personal computer and the final spectrum is output on both a printer and an X–Y plotter.

XPS AND ISEELS RESULTS

The valence-band XPS spectra of $Cu_x(CeS)_{1.16}(NbS_2)_2$, $Cu_x(SmS)_{1.16}(NbS_2)_2$, and $(SmS)_{1.19}NbS_2$ are compared in Fig. 2. The XPS spectrum of $(SmS)_{1.19}NbS_2$ has already been discussed in the previous paper (22). According to the result, the lower valence bands centered at 13 eV are derived from S 3s orbitals and the upper valence bands are primarily from S 3p orbitals although the XPS structures overlap the multiplet structures in the higher binding energy region, which are derived from Sm^{3+} $4f^4$ final states. As Cu is intercalated, the intensities around 3 eV increase owing to Cu 3d states and a shoulder just below the photoemission threshold, which arises from occupied Nb $4d_{z^2}$ states, enlarges due to charge transfer from intercalated Cu atoms to NbS$_2$ layers. Here we recall that Cu-intercalated misfit-layer

compounds crystallize in such a way that every second MS layer of the first-stage misfit-layer compound is substituted by a Cu layer. Taking the crystal structure and the enhancement of the threshold structure into account, we may conclude that a larger number of electrons are transferred from a Cu layer than from a SmS layer. Electrical studies of $(SmS)_{1.19}NbS_2$ (23, 24) and $(SmS)_{1.19}$ TaS_2 (25) show that ca. 0.9 electrons per transition-metal atom are transferred from SmS layers to TS_2 (T = Nb and Ta) layers. Thus the valence-band XPS spectra indicate that each Cu atom donates more than 1.3 electrons to NbS$_2$ layers. However, the Cu 2p XPS spectra in Fig. 3 give no evidence for the existence of Cu^{2+} ions.

For cupric compounds such as CuS and CuO, the Cu 2p XPS spectra exhibit satellite structures on the higher binding energy sides of the spin–orbit-split $2p_{3/2}$ and $2p_{1/2}$ peaks. These satellite structures are considered to be caused by interconfiguration interaction of the XPS final states (26–30). Cu^{2+} has an empty 3d state in the initial state, which can be filled with an extra electron transferred from neighboring ligands. In this case, two different final states are possible by interconfiguration interaction at the presence of a core hole. The poorly screened final state of $2p^5 3d^9$ produces the satellite structures and the well-screened final state of $2p^5 3d^{10} L^{-1}$ provides the main peak, where L^{-1}
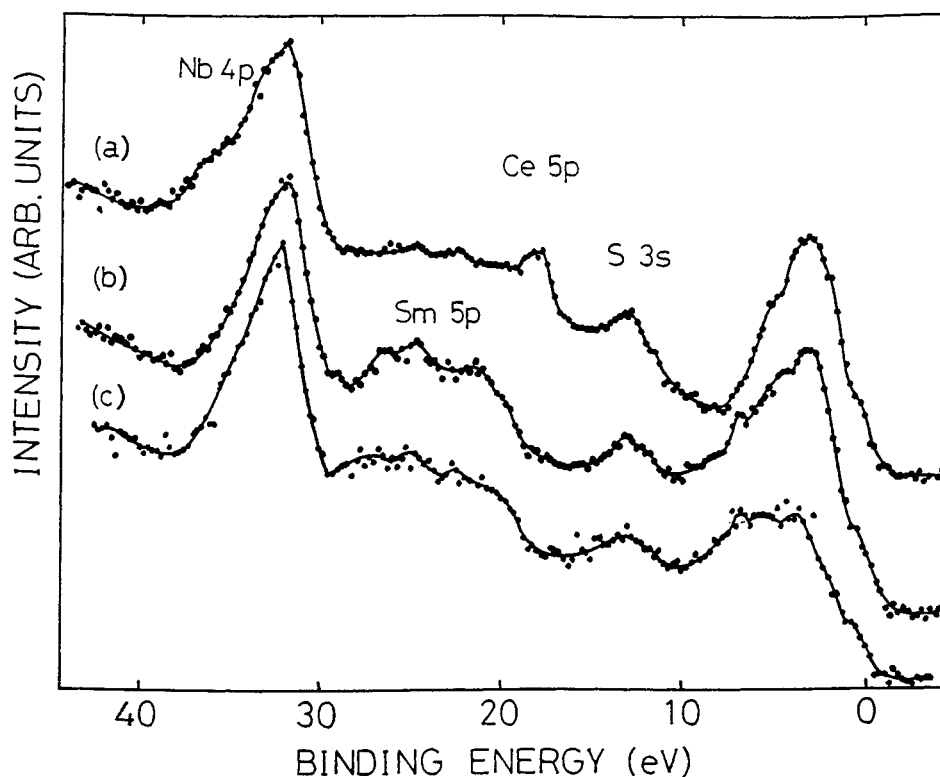

FIG. 2. Valence-band and shallow core XPS spectra: (a) $Cu_x(CeS)_{1.16}(NbS_2)_2$, (b) $Cu_x(SmS)_{1.16}(NbS_2)_2$, and (c) $(SmS)_{1.19}NbS_2$.
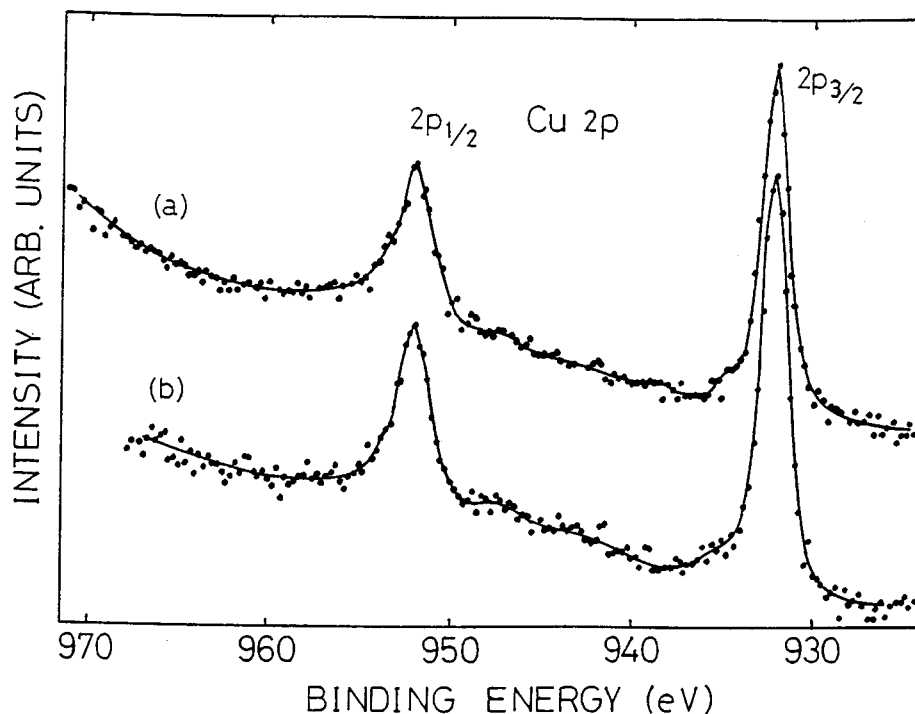
FIG. 3. Cu 2p XPS spectra: (a) $Cu_x(NbS)_{1.16}(NbS_2)_2$ and (b) $Cu_x(SmS)_{1.16}(NbS_2)_2$.

denotes a hole in the ligand-derived valence band. Such electron transfer does not occur in cuprous compounds containing Cu^+, because the ground state has no empty d states. (Here it is worth noting that although the Novakov spectrum (26) for Cu_2O as well as for cupric compounds exhibits large satellites, the result presents a striking contrast with the results of Rosencwaig and Wertheim (27) and Ishii *et al.* (31), which reveal only faint structures in the energy regions.) Our XPS spectra are quite similar to that of Cu metal (32) with no satellites, suggesting that intercalated Cu atoms exist as monovalent ions, in contrast with the valence-band result. Presently, we have no experimentally or theoretically supported explanation for the disagreement, although other charge donation centers are considered due to the presence of interstitial Cu atoms and other lattice defects. We should also consider strong hybridization between Cu 3d and Nb $4d_{z^2}$ states. If a Nb $4d_{z^2}$ orbital extends to a Cu atom, strong hybridization and the reconstruction of the energy band structure are expected. The Nb 4p XPS spectrum of $Cu_x(SmS)_{1.16}(NbS_2)_2$ reveals an additional structure around 4.4 eV above the main peak (see Fig. 2a) and some other evidence for Cu–Nb interaction exists. This evidence is discussed later.

Next, we consider the intercalation effect on the MS layers. The Ce and Sm 3d XPS spectra of $Cu_x(MS)_{1+y}$ $(NbS_2)_2$ $(M = Ce$ and Sm) have been compared with those of $(MS)_{1+y}NbS_2$. The binding energies of the main features are tabulated in Table 1. As discussed in the previous paper

TABLE 1

Binding Energies in eV of the Main Features of the XPS Spectra of $Cu_x(CeS)_{1+y}(NbS_2)_2$, $Cu_x(SmS)_{1+y}(NbS_2)_2$, and $(SmS)_{1+y}NbS_2$

$Cu_x(CeS)_{1+y}(NbS_2)_2$	$Cu_x(SmS)_{1+y}(NbS_2)_2$	$(SmS)_{1+y}NbS_2$	Assignment
0.5	0.5	0.5	Nb d_{z^2}
3.0	3.0		Cu 3d
		3.8	
5.0	5.0	5.0	
	6.8	6.8	Sm^{3+} 4f
	8.3	8.3	
13.0	13.0	13.0	S 3s
18.0			Ce 5p
	20.0	20.0	Sm 5p
22.5		22.5	$MgK\alpha_{3,4}$
25.0	25.0	25.0	
	26.7	27.5	
31.8	31.8	32.0	Nb 4p
36.2			
881.3			Ce $3d_{5/2}$ $4f^2$
885.5			$4f^1$
899.7			Ce $3d_{3/2}$ $4f^2$
903.8			$4f^1$
932.0	932.0		Cu $2p_{3/2}$
934.8	935.3		
952.0	952.0		Cu $2p_{1/2}$
	1074.0	1074.0	$MgK\alpha_{3,4}$
	1083.0	1083.5	Sm $3d_{5/2}$
		1091.0	
	1110.5	1110.5	Sm $3d_{3/2}$
	1113.0	1113.5	
	1116.0	1116.0	

(18), the Ce $3d$ XPS spectrum of $(CeS)_{1.16}NbS_2$ shows the main peak and the pre-edge structures which are, respectively, assigned to the poorly screened Ce^{3+} $3d^9$ $4f^1$ final state and the well-screened $3d^9$ $4f^2$ L^{-1} final state. Comparison of the Ce $3d$ XPS spectra of $Cu_x(CeS)_{1.16}(NbS_2)_2$ and $(CeS)_{1.16}NbS_2$ shows that the probability of having an f electron in the ground state as well as the coupling energy Δ is not changed from that of the pristine compound (33). The Sm $3d$ XPS spectra of $Cu_x(SmS)_{1.19}(NbS_2)_2$ and $(SmS)_{1.19}NbS_2$ show the well-separated $3d_{5/2}$ and $3d_{3/2}$ components. The spectra are quite similar to each other as shown in Fig. 4. The main peak of each spin–orbit-split component is attributed to the Sm^{3+} $3d^9$ $4f^5$ final state and a shoulder on the higher binding energy side of the $3d_{3/2}$ peak is attributed to the multiplet structures which are caused by LS coupling. Detailed assignments have been made in the previous paper (22). Finally, all the experimental results obtained suggest that the chemical environment within an MS layer is not changed by Cu intercalation and that rare-earth metal atoms exist as trivalent ions.

Figure 5 shows the Nb $N_{2,3}$ ISEELS spectra of $Cu_x(MS)_{1+y}(NbS_2)_2$, $(MS)_{1+y}NbS_2$, and related compounds, which represent the empty Nb $4d$ states. $[Cu_xNbS_2]_z[(SnS)_{1.17}NbS_2]_{1-z}$ is a composite crystal containing the different crystal parts of Cu_xNbS_2 and $(SnS)_{1.17}NbS_2$. These spectra have a common nature, re-flecting the local and partial density of states around an excited Nb atom. The first peak around 31.5 eV is assigned to unoccupied Nb $4d_{z^2}$ states. The integrated intensity, which gives a rough estimation of the number of unoccupied Nb $4d_{z^2}$ states, decreases in the sequence of $(CeS)_{1.16}(NbS_2)_2$, $(CeS)_{1.16}NbS_2$, Cu_xNbS_2, and $Cu_x(CeS)_{1.16}(NbS_2)_2$. The result supports the earlier XPS conclusions that charge transfer occurs from Cu to NbS_2 layers and that the *effective* number of transferred electrons is larger for a Cu layer at high concentration than for a CeS layer. The second and third peaks are attributed to upper d and higher sp conduction bands, respectively. It is also found that the near-edge structures are not changed appreciably upon Cu intercalation. This fact suggests that the energy band structures may be discussed within the rigid-band model. In contrast, spectrum a in Fig. 5 shows a large peak at the threshold and the higher energy tail overlaps the second peak. In this case, we may regard that the energy band structure, especially the d bands, is varied and that the rigid-band model is no longer valid. A similar phenomenon is observed in the S $L_{2,3}$ ISEELS spectrum of $Cu_x(CeS)_{1.16}(NbS_2)_2$. It is surprising that the ISEELS measurements for $Cu_x(CeS)_{1.16}(NbS_2)_2$ give two different kinds of S $L_{2,3}$ spectra. In Fig. 6 they are compared with the S $L_{2,3}$ ISEELS spectra of $2H$-TaS_2 with a half-filled d_{z^2} band and MoS_2 with a completely filled d_{z^2} band. A sharp peak appears at the threshold for
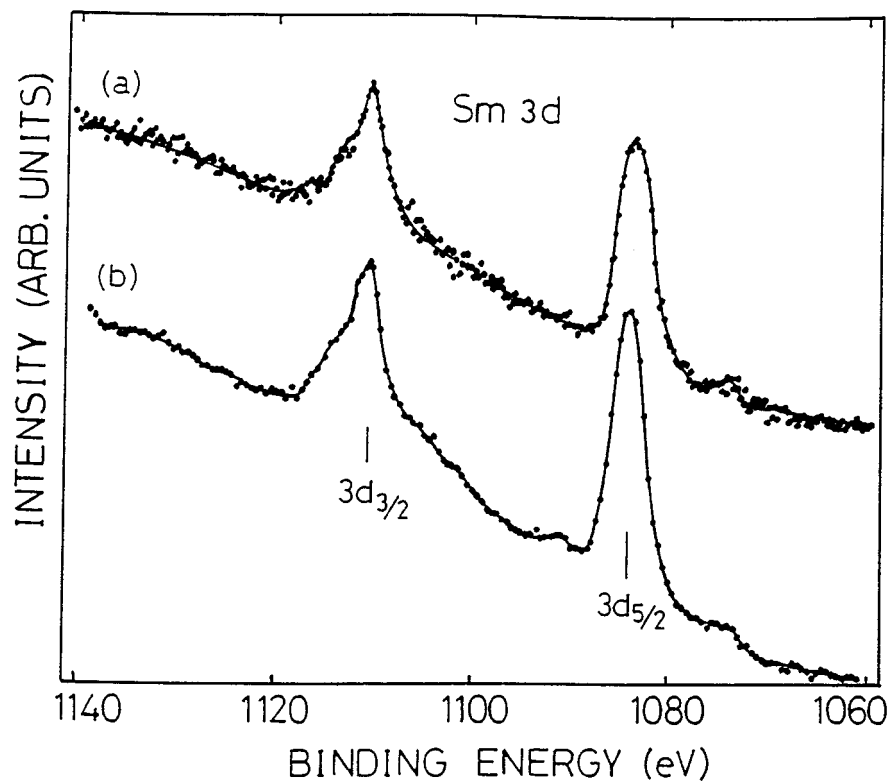

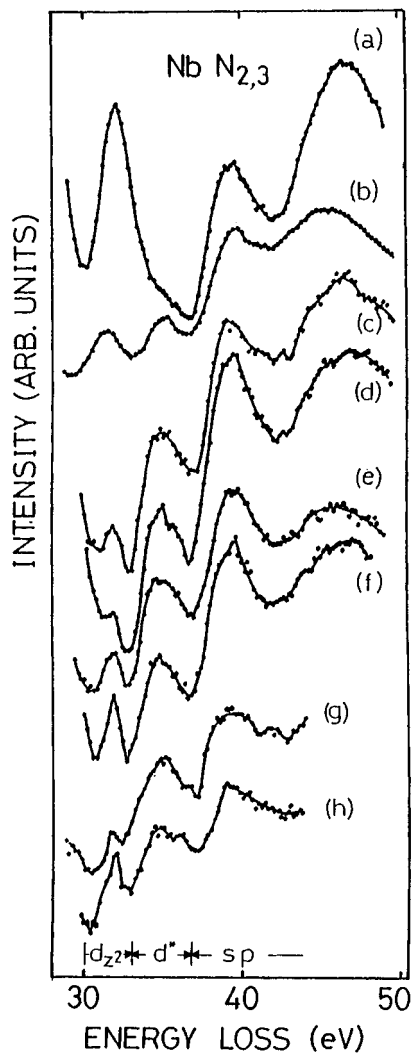**FIG. 4.** Sm $3d$ XPS spectra: (a) $Cu_x(SmS)_{1.16}(NbS_2)_2$ and (b) $(SmS)_{1.19}NbS_2$.

FIG. 5. Nb $N_{2,3}$ ISEELS spectra: (a) $Cu_x(SmS)_{1.16}(NbS_2)_2$, (b) $(SmS)_{1.19}NbS_2$, (c) Cu_xNbS_2, (d) $Cu_x(CeS)_{1.16}(NbS_2)_2$, (e) $(CeS)_{1.16}NbS_2$, (f) $(CeS)_{1.16}(NbS_2)_2$, (g) $[Cu_xNbS_2]_z(SnS)_{1.17}NbS_2]_{1-z}$, and (h) $(SnS)_{1.17}NbS_2$.

FIG. 6. S $L_{2,3}$ ISEELS spectra of $Cu_x(CeS)_{1.16}(NbS_2)_2$, MoS_2, and $2H$-TaS_2. Spectra a and b were obtained from different crystals of $Cu_x(CeS)_{1.16}(NbS_2)_2$.

$2H$-TaS_2. This peak represents the partial density of empty states of the half-filled d_{z^2} band. Such a sharp peak is not found for MoS_2, because the d_{z^2} band is completely filled with two electrons per metal atom. A large peak on the higher energy side, which has been attributed to the upper d bands, shifts to lower energy in MoS_2 than in TaS_2. This shift is due to the chemical shift of a core $2p$ level and/or the lower energies of the upper d bands. Since the electronic structure of NbS_2 is quite similar to that of $2H$-TaS_2 (34), we may expect a sharp peak at the threshold. The spectrum of $Cu_x(CeS)_{1.16}(NbS_2)_2$ in Fig. 6a reveals no sharp peak but does reveal a shoulder on the lower energy side of a large peak. Except for the reduced intensity of its shoulder, the overall appearance of the near-edge structures is rather
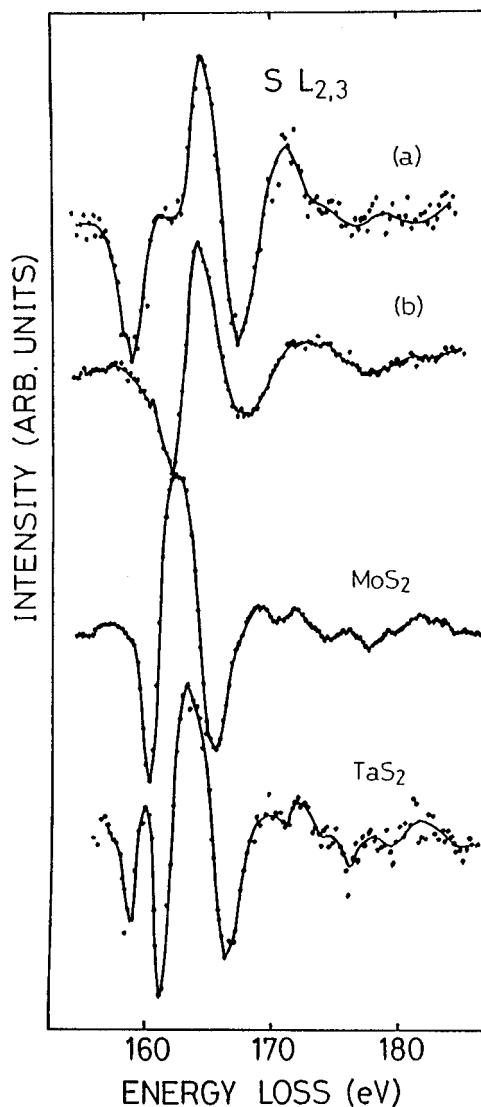
similar to that of the S $L_{2,3}$ ISEELS spectrum of ZrS_2, which shows double peaks arising from the t_{2g} and e_g bands just above the threshold. Here we recall that ZrS_2 belongs to the family of layered IVA transition-metal dichalcogenides in which transition-metal atoms are coordinated octahedrally to six S atoms whereas each transition-metal atom in NbS_2, $2H$-TaS_2, and MoS_2 sits in the center of a trigonal prism with six S atoms at the corners. If the coordination changes from trigonal-prismatic coordination to octahedral coordination, the d band structure is strongly affected so that the rigid-band model is no longer valid. The following gives a brief discussion for the case of TaS_2. It is well-known that Ta atoms in $1T$- and $2H$-TaS_2 have different coordinations, i.e., octahedral coordination for $1T$-TaS_2 and
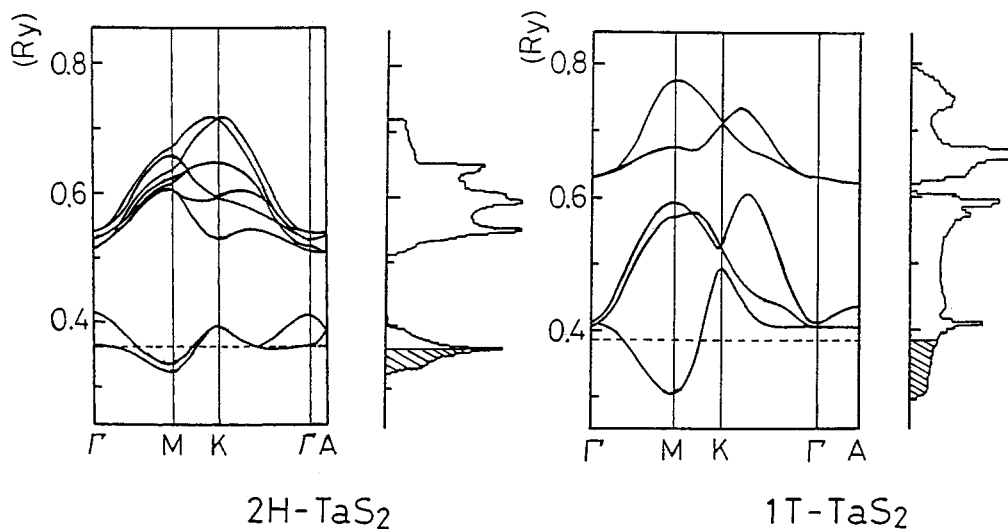
FIG. 7. Ta $5d$ band structures and the densities of states of $2H$- and $1T$-TaS$_2$, which were calculated by Mattheiss (35). Broken lines show the Fermi level.

trigonal-prismatic coordination for $2H$-TaS$_2$. Their energy band structures and the densities of states, which have been calculated by Mattheiss (35), are reproduced in Fig. 7. As can be seen from the calculations, the d_{z^2} band, which is the lowest conduction band for $2H$-TaS$_2$, is separated from the upper d bands by a distinct energy gap due to strong d–d hybridization, whereas the d bands for $1T$-TaS$_2$ are split into lower t_{2g} (d_{z^2}, $d_{x^2-y^2}$, and d_{xy}) and upper e_g (d_{xz} and d_{yz}) bands by the crystal field. Since the occupation numbers of the d_{z^2} and the t_{2g} bands are 2 and 6 per Ta atom, respectively, then the lowest conduction band is completely filled with an additional one and five electrons for $2H$- and $1T$-TaS$_2$, respectively. As a result, for $1T$-TaS$_2$ more than one electron can be donated from the intercalated species to the lowest conduction band unlike $2H$-TaS$_2$. In other words, if TaS$_2$ possesses more than two d electrons per Ta atom, the $1T$ polytype would be more stable in energy than the $2H$ polytype. Similarly, if more than one electron is transferred to NbS$_2$ layers, octahedral coordination would be more stable than trigonal-prismatic coordination, resulting in a phase transition. Consequently, the spectra of Cu$_x$(CeS)$_{1.16}$(NbS$_2$)$_2$ show two different kinds of spectra; one reveals near-edge structures similar to those observed for ZrS$_2$ and $1T$-TaS$_2$ and the other shows structures similar to those observed for $2H$-TaS$_2$ and MoS$_2$. Figure 6b exhibits a reduced d_{z^2} peak, and other structures remain almost unchanged from those of $2H$-TaS$_2$ and MoS$_2$. In this case, the rigid-band model would be a useful model in interpreting electrical and optical properties. The reduction of the d_{z^2} peak in Fig. 6b as well as the t_{2g} peak in Fig. 6a is explained in terms of charge transfer from Cu and CeS layers.

Recently, Koslowski et al. (36) have shown from scanning tunneling microscope (STM) study of Ag-intercalated

NbSe$_2$ that the stacking order of NbSe$_2$ layers changes from the $2H$ polytype to the $1T$ polytype near the surface and charge-density-wave (CDW) transitions occur at room temperature. Our experimental results show that the rigid-band model is no longer valid for samples containing a large number of intercalated Cu atoms and the d band structure is drastically changed through the phase transition within a NbS$_2$ layer. Now we consider the crystal structure of the Cu-intercalated misfit-layer compounds. Four different polytypes are proposed. They are shown schematically in Fig. 8. The polytype in Fig. 8a has been found by Meerschaut et al. (11) and by Terashima (19) in second-stage misfit-layer compounds. In the polytype two adjacent NbS$_2$ layers are identical to those of $3R$-NbS$_2$ and each Nb atom sits in the center of a trigonal prism with six S atoms at the corners. The unit cell is monoclinic, so that the c axis does not coincide with the direction perpendicular to the layers. The polytype in Fig. 8b contains the same NbS$_2$ layers as observed in $2H$-MoS$_2$. Here, it is worth noting that the crystal structure of Cu$_x$NbS$_2$ changes from the NbS$_2$ type to the MoS$_2$ type near the maximum x value (37). The phase transition leads to shorter intermetallic bonding between Cu and Nb atoms by locating a Cu atom just above and below a Nb atom. The reduced Cu–Nb distance, which leads to a stronger Cu–Nb interaction, is also accessible for polytypes shown in Fig. 8c, and d. In the polytype in Fig. 8c, all Nb atoms are coordinated octahedrally to six S atoms. TS$_2$ layers like this have been found in $3R$-TaS$_2$ (38, 39). The polytype in Fig. 8d contains Nb atoms, half with octahedral coordination and half with trigonal-prismatic coordination. Similar TS$_2$ layers have been found in $4H$-NbSe$_2$ (40).
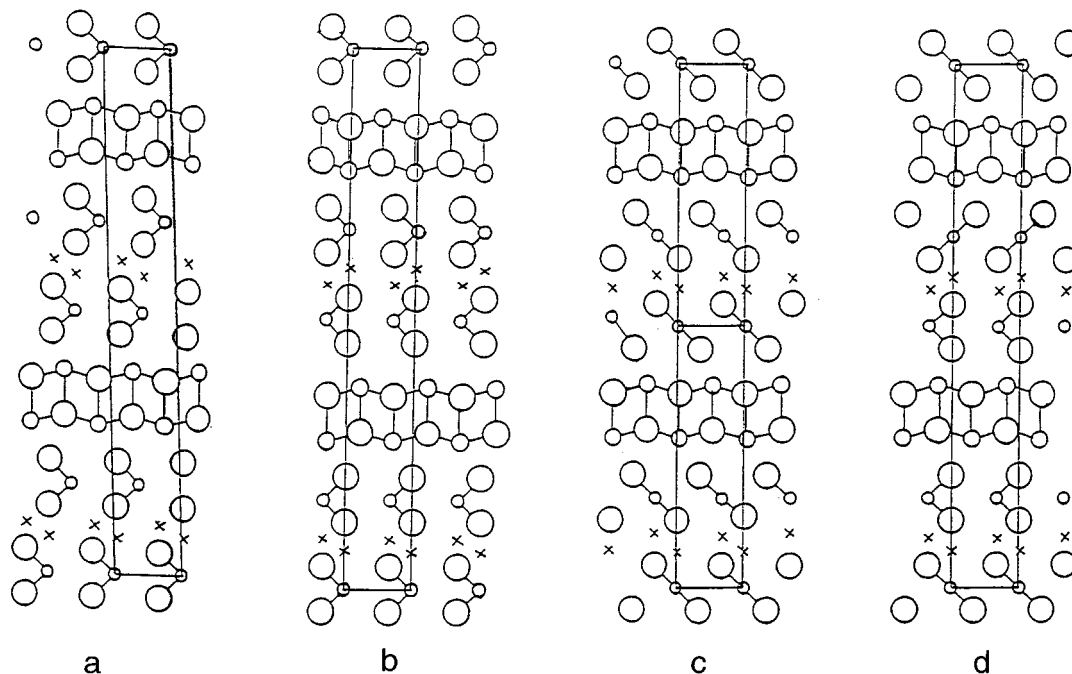
FIG. 8. Schematic diagrams of four different polytypes which are proposed for Cu-intercalated misfit-layer compounds. Solid lines show a unit cell.

EELS RESULTS

Figures 9 and 10 show the EELS spectra of several different crystals for $Cu_x(CeS)_{1.16}(NbS_2)_2$ and related compounds. For comparison, the energies of the main features are tabulated in Table 2. It is found that a small difference in the number of intercalated Cu atoms causes systematic variations in interband transitions and excitation of plasmons. The loss structures are classified into two groups. One is the loss structures observed in the pristine compound. They have already been discussed in the previous paper (22). The other is new loss-structures generated by Cu intercalation. The loss structures at energies less than 3.5 eV are connected to interband transitions from the occupied Nb d_{z^2} states to the upper Nb 4d bands. A loss peak at 5.0 eV, which can only be observed in the higher energy resolution spectra at incident energies less than 50 eV, is attributed to Ce 4f–5d transitions and a peak at 5.5 eV is ascribed to S 3p–Ce 5d transitions within a CeS layer and S 3p-Nb 4d transitions within a NbS$_2$ layer although for Cu_x $(CeS)_{1.16}(NbS_2)_2$ a considerable contribution of Cu 3d states exists. It is found in Fig. 10a and b that the interband transitions are changed significantly from those of the pristine compound. A peak at 8 eV arises from partial plasma resonance which occurs when interband transitions to Nb 4d bands are exhausted. A large peak around 22 eV arises from a bulk plasma oscillation within a NbS$_2$ layer. These plasmon peaks diminish at higher Cu concentration. In contrast, a surface plasmon observed at 13 eV grows upon Cu intercalation. It is found that the intensity is much smaller than that of the bulk plasmon in the pristine compound, although they are comparable in the Cu-intercalated misfit-layer compound. The enhancement of a surface plasmon may be connected to the three-dimensionality of the Cu-intercalated compound. The other structures are shoulders observed on the lower and higher energy sides of a bulk plasmon peak, which are caused by electron transitions from S 3s and Ce 5p levels, respectively, and fine loss structures at energies greater than 31 eV, which are caused by the Nb $N_{2,3}$ transitions.
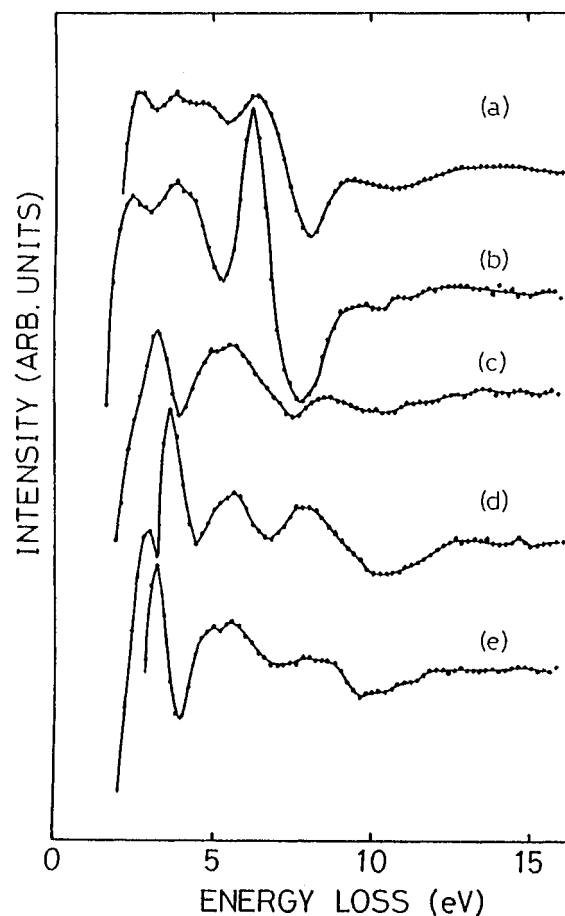
The spectra in Figs. 9e and 10c for $Cu_x(CeS)_{1.16}(NbS_2)_2$ are quite similar to those of the pristine compound, suggesting that the electronic structure of this sample remains almost unchanged upon Cu intercalation and the rigid-band model is still valid. In this case, the energy band structure is discussed, based on the simple superposition of energy bands of each composite layer. The spectra in Figs. 9a and 10a are, on the other hand, quite different from those of the pristine compound. In this case, the rigid-band model is no longer valid. A new peak appears at 27 eV. The peak energy is almost independent of the incident energy and momentum transfer. Unfortunately, we have no reasonable explanation for this peak. The free-electron value of a bulk plasmon within a $Cu_x(NbS_2)_2$ layer
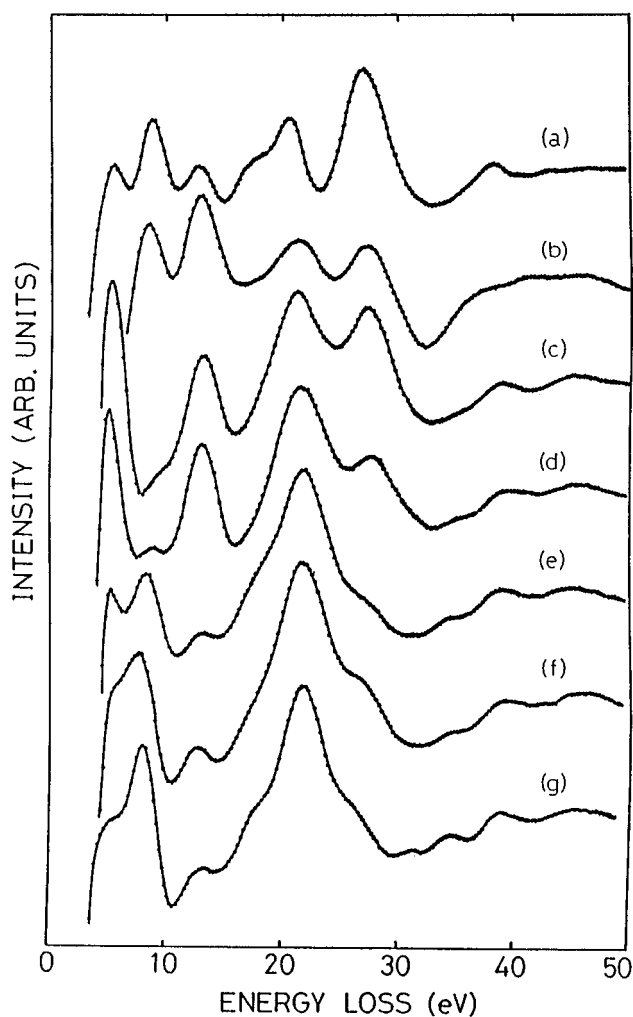
FIG. 9. EELS spectra of (a–e) several different crystals of $Cu_x(CeS)_{1.16}$ $(NbS_2)_2$, (f) $(CeS)_{1.16}(NbS_2)_2$, and (g) $(CeS)_{1.16}NbS_2$. The spectra measured at an incident energy of 350 eV and a modulation voltage of 2 V.

FIG. 10. High energy resolution EELS spectra of (a–c) several different crystals of $Cu_x(CeS)_{1.16}(NbS_2)_2$, (d) $(CeS)_{1.16}(NbS_2)_2$, and (e) $(CeS)_{1.16}$ NbS_2. The samples for (a), (b), and (c) are the same as those used for the measurements in (a), (c), and (e) of FIG. 9, respectively. The spectra were obtained at an incident energy of 70 eV and a modulation voltage of 0.5 V.
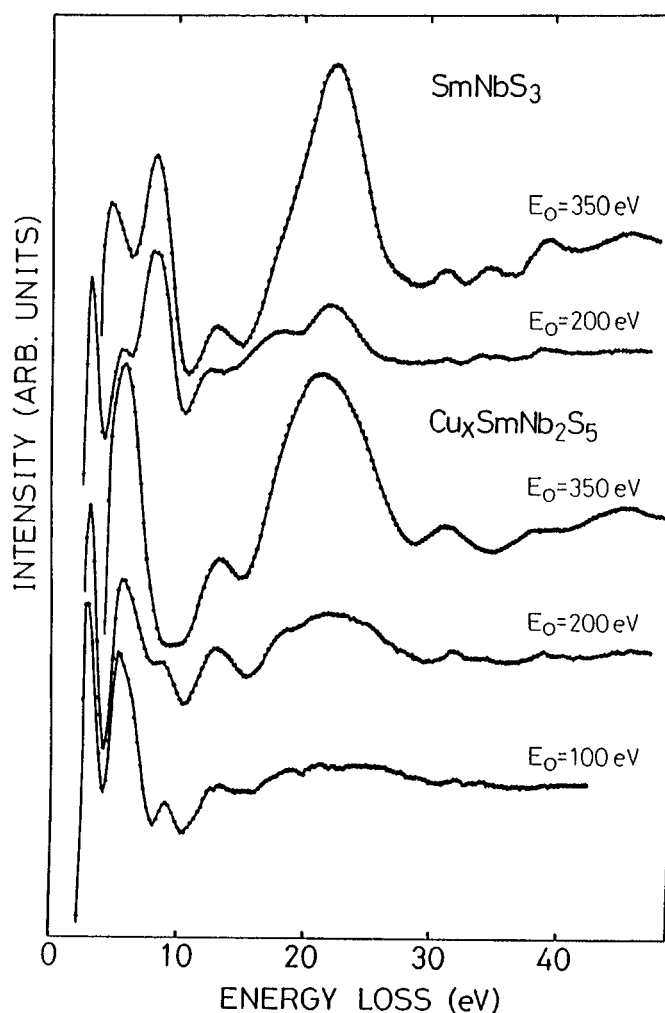
is ca. 22 eV even if 10 Cu $3d$ and 1 Cu $4s$ electrons participate in excitation of the bulk plasmon. This value is much smaller than the experimental value. The Ce $O_{2,3}$ structures must be considered because they appear in this energy region, although the peak intensities which are expected from the oscillator strengths are much smaller. Then the peak may be attributed to a new plasma oscillation. Further studies are necessary to understand the origin of the new peak. Despite the presence of the undefined new peak, the EELS results suggest that the phase transition occurs at high Cu concentration, consistent with the XPS and ISEELS results. The apparently continuously changed EELS structures show that real crystals contain multiple polytypes and the overall spectral shape depends strongly on Cu concentrations and inhomogeneous Cu distribution.

Figure 11 shows the EELS spectra of $Cu_x(SmS)_{1.16}$ $(NbS_2)_2$ at different incident energies, which are compared with those of $(SmS)_{1.19}NbS_2$. A partial plasma resonance peak at 8.2 eV diminishes as well as $Cu_x(CeS)_{1.16}(NbS_2)_2$ and a bulk plasmon peak around 22 eV broadens. In this case, however, a new plasma oscillation is not clearly found.

CONCLUSIONS

In layered transition-metal dichalcogenides, d covalency provides a stabilizing factor for the trigonal-prismatic coordination found in the group VI and V compounds and a more symmetric electrostatic field is favored for the octahedral coordination found in the group IV and V compounds and in one group VI compound. Consequently, trigonal-prismatic coordination is adopted in more covalent

TABLE 2

Energies in eV of the Main Features of the EELS Spectra of $Cu_x(Ces)_{1+y}(NbS_2)_2$, $Cu_x(Sms)_{1+y}(NbS_2)_2$, $Cu_x(SnS)_{1+y}(NbS_2)_2$, $(Ces)_{1+y}(NbS_2)_2$, $(SmS)_{1+y}NbS_2$, and Cu_xNbS_2

$Cu_x(CeS)_{1+y}(NbS_2)_2$		$Cu_x(SmS)_{1+y}(NbS_2)_2$	$Cu_x(SnS)_{1+y}(NbS_2)_2$	$(CeS)_{1+y}(NbS_2)_2$	$(SmS)_{1+y}NbS_2$	Cu_xNbS_2
2.5						
3.2	3.8	2.9	3.0	3.5	3.0	3.2
5.0	4.7					
5.5		5.5	5.2	5.5	5.5	5.3
	6.3	6.0				
			7.0			
8.0				8.0	8.2	8.0
	9.0	9.0				9.0
	13.0	13.0	12.0	12.7	12.7	12.5
	17.5	17.5	17.3	16.5	17.5	17.5
		18.8		18.7		18.8
	21.3	21.5	21.4	22.0	22.3	22.0
			26.5			
	27.3			27.5		
31.3		31.3	31.3	31.3	31.3	31.3
34.3		34.0	33.8	34.7	34.5	34.0
38.5	38.3	38.0	39.0	39.0	39.0	38.2
45.0		45.3	45.0	46.0	46.0	

bonding whereas octahedral coordination is adopted in more ionic bonding. This paper gives evidence for the phase transition of Cu-intercalated misfit-layer compounds which results in the change of the coordination of Nb atoms from the trigonal-prismatic to the octahedral one. The phase transition results from the charge transfer from intercalated Cu atoms to NbS_2 layers. If more than one electron per Nb atom is transferred to NbS_2 layers, the d_{z^2} band is completely filled and residual transferred electrons move into the upper d bands. In this case, octahedral coordination is more stable than trigonal-prismatic coordination because the lowest conduction bands allow a larger number of electrons. Then as discussed earlier, octahedral coordination is more favorable than trigonal-prismatic coordination at high Cu concentration and the phase transition occurs near the maximum uptake, resulting in a shorter Cu–Nb distance, which in turn results in a stronger Cu–Nb interaction. Finally, we propose four polytypes with different NbS_2 sublattices for the Cu-intercalated misfit-layer compounds, that is, the $3R$-NbS_2 type, the $2H$-MoS_2 type, the $2H$-modulated $3R$-TaS_2 type, and the $4H$-$NbSe_2$ type. The former two sublattices contain Nb atoms with trigonal-prismatic coordination, the third sublattice contains Nb atoms with octahedral coordination, and the last sublattice contains Nb atoms with both coordinations, half with trigonal-prismatic coordination and half with octahedral coordination.

FIG. 11. EELS spectra of $Cu_x(SmS)_{1.19}(NbS_2)_2$ and $(SmS)_{1.19}NbS_2$ at different incident energies. In the figure, $Cu_x(SmS)_{1.19}(NbS_2)_2$ and $(SmS)_{1.19}NbS_2$ are denoted $Cu_xSmNb_2S_5$ and $SmNbS_3$, respectively.

REFERENCES

1. W. Sterzel, *Naturwissenschaften* **53,** 199 (1966); W. Sterzel and J. Horn, *Z. Anorg. All. Chem.* **376,** 254 (1970).
2. L. Schmidt, *Phys. Lett. A* **31,** 551 (1970); L. Schmidt, S. L. McCarthy, and J. P. Maita, *Solid State Commun.* **8,** 1513 (1970).
3. L. Otero-Diaz, J. D. FitzGerald, T. B. Williams, and B. G. Hyde, *Acta Crystallogr. B* **41,** 405 (1985).
4. G. A. Wiegers, A. Meetsma, R. J. Haange, and J. L. de Boer, *Mater. Res. Bull.* **23,** 1551 (1988).
5. A. Meerschaut, P. Rabu, and J. Rouxel, *C. R. Acad. Sci. Paris* **307,** 1513 (1988).
6. T. B. Williams and B. G. Hyde, *Acta Crystallogr. B* **44,** 467 (1988).
7. G. A. Wiegers and A. Meerschaut, *Mater. Sci. Forum* **100/101,** 101 (1992).
8. S. van Smaalen, *Mater. Sci. Forum* **100/101,** 173 (1992).
9. S. Kuypers and J. van Landuyt, *Mater. Res. Forum* **100/101,** 223 (1992).
10. G. A. Wiegers, *Prog. Solid State Chem.* **24,** 1 (1996).
11. L. Guemas, P. Rabu, A. Meerschaut, and J. Rouxel, *Mater. Res. Bull.* **23,** 1061 (1988); A. Meerschaut, L. Guemas, C. Auriel, and J. Rouxel, *Eur. J. Solid State Inorg. Chem.* **27,** 557 (1990); C. Auriel, A. Meerschaut, R. Roesky, and J. Rouxel, *Eur. J. Solid State Inorg. Chem.* **29,** 1079 (1992); C. Auriel, A. Meerschaut, and J. Rouxel, *Mater. Res. Bull* **28,** 675 (1993); R. Roesky, A. Meerschaut, J. Rouxel and J. Chen, *Z. Anorg. Allg. Chem.* **619,** 117 (1993); L. M. Hoistad, A. Meerschaut, P. Bonneau, and J. Rouxel, *J. Solid State Chem.* **114,** 435 (1995).
12. Y. Oosawa, Y. Gotoh, and M. Onoda, *Chem. Lett.* 1563 (1989); Y. Gotoh, M. Onoda, J. Akimoto, and Y. Oosawa, *Jpn. J. Appl. Phys.* **30,** L1039 (1991); Y. Oosawa, Y. Gotoh, J. Akimoto, T. Tsunoda, M. Sohma, and M. Onoda, *Jpn. J. Appl. Phys.* **31,** L1096 (1992).
13. L. Hernán, J. Morales, J. Pattanayak, and J. L. Tirado, *Chem. Lett.* 1981 (1991).
14. W. Y. Zhou, A. Meetsma, J. L. de Boer, and G. A. Wiegers, *Mater. Res. Bull.* **27,** 563 (1992).
15. M. Saeki, M. Onoda, and M. Ohta, *Mater. Res. Bull.* **28,** 279 (1993).
16. L. Hernán, P. Lavela, J. Morales, J. Pattanayak, and J. L. Tirado, *Mater. Res. Bull.* **26,** 1211 (1991); L. Hernán, J. Morales, J. Pattanayak, and J. L. Tirado, *J. Solid State Chem.* **100,** 262 (1992); L. Hernán, J. Morales, L. Sánchez, and J. L. Tirado, *Solid State Ionics* **58,** 179 (1992); C. Barriga, P. Lavela, J. Morales, J. Pattanayak, and J. L. Tirado, *Chem. Mater.* **4,** 1021 (1992); P. Lavela, J. Morales, and J. L. Tirado, *Chem. Mater.* **4,** 2 (1992).
17. C. Auriel, A. Meerschaut, P. Deniard, and J. Rouxel, *C. R. Acad. Sci. Paris* **313,** 1225 (1991); P. Bonneau, J. L. Mansot, and J. Rouxel, *Mater. Res. Bull.* **28,** 757 (1993).
18. Y. Ohno, *Phys. Rev. B* **54,** 11693 (1996).
19. T. Terashima, Thesis, Kyoto University, 1993.
20. A. E. van Arkel and C. Crevecoeur, *J. Less-Common Met.* **5,** 177 (1963).
21. J. M. Voorhoeve-van den Berg, *J. Less-Common Met.* **26,** 399 (1972).
22. Y. Ohno, *J. Phys. Condens. Matter* **4,** 7815 (1992).
23. A. Meerschaut, C. Auriel, A. Lafond, C. Deudon, P. Gressier, and J. Rouxel, *Eur. J. Solid State Inorg. Chem.* **28,** 581 (1991).
24. R. J. Cava, B. Batlogg, R. B. van Dover, A. P. Ramirez, J. J. Krajewski, W. F. Peck, Jr, and L. W. Rupp, Jr., *Phys. Rev. B* **49,** 6343 (1994).
25. G. A. Wiegers, A. Meetsma, R. J. Haange, and J. L. de Boer, *J. Less-Common Met.* **168,** 347 (1991).
26. T. Novakov, *Phys. Rev. B* **3,** 2693 (1971).
27. A. Rosencwaig and G. K. Wertheim, *J. Electron Spectrosc.* **1,** 493 (1973).
28. G. van der Laan, C. Westra, C. Haas, and G. A. Sawatzky, *Phys. Rev. B* **23,** 4369 (1981).
29. K. Okada and A. Kotani, *J. Phys. Soc. Jpn.* **58,** 2578 (1989).
30. A. E. Bocquet, T. Mizokawa, T. Saitoh, H. Namatame, and A. Fujimori, *Phys. Rev. B* **46,** 3771 (1992).
31. H. Ishii, T. Koshizawa, T. Hanyu, and S. Yamaguchi, *Jpn. J. Appl. Phys.* **32,** 1070 (1993).
32. C. D. Wagner, W. M. Riggs, L. E. Davis, J. F. Moulder, and G. E. Muilenberg, *in* "Handbook of X-Ray Photoelectron Spectroscopy" (G. E. Muilenberg, Ed.), p. 82. (Perkin–Elmer, Minnesota, 1979).
33. Y. Ohno, *Phys. Rev. B* **48,** 5515 (1993).
34. C. Y. Fong and M. Schlüter, *in* "Electrons and Phonons in Layered Crystal Structure" (T. J. Wieting and M. Schlüter, Eds.), p. 145. Reidel, Boston, 1979.
35. L. F. Mattheiss, *Phys. Rev. B* **8,** 3719 (1973).
36. B. Koslowski, W. Xu, B. Blackfold, and M. H. Jericho, *Phys. Rev. B* **54,** 11706 (1996).
37. R. de Ridder, G. van Tendeloo, J. van Landuyt, D. van Dyck, and S. Amelinckx, *Phys. Status Solidi A* **37,** 591 (1976); G. van Tendeloo, R. de Ridder, D. van Dyck, J. van Landuyt, and S. Amelinckx, *Phys. Status Solidi A* **38,** 185 (1976); R. de Ridder, D. van Dyck, G. van Tendeloo, J. van Landuyt, and S. Amelinckx, *Phys. Status Solidi A* **39,** 383 (1977).
38. F. Jellinek, *J. Less-Common Met.* **4,** 9 (1962).
39. R. M. A. Lieth and J. C. J. M. Terhell, *in* "Preparation and Crystal Growth of Materials with Layered Structures" (R. M. A. Lieth, Ed.), p. 141. Reidel, Boston, 1977.
40. F. Kadijk and F. Jellinek, *J. Less-Common Met.* **23,** 437 (1971).